Corrosion Science 92 (2015) 69–75

Contents lists available at ScienceDirect

Corrosion Science

journal homepage: www.elsevier.com/locate/corsci

Impact of electrolyte intercalation on the corrosion of graphene-coated copper

I. Wlasny [a,*], P. Dabrowski [b], M. Rogala [a], I. Pasternak [b], W. Strupinski [b], J.M. Baranowski [b], Z. Klusek [a]

[a] Department of Solid State Physics, Faculty of Physics and Applied Informatics, University of Lodz, Pomorska 149/153, Lodz 90-236, Poland
[b] Institute of Electronic Materials Technology, Wolczynska 133, Warsaw 01-919, Poland

ARTICLE INFO

Article history:
Received 5 June 2014
Accepted 15 November 2014
Available online 21 November 2014

Keywords:
B. AES
A. Copper
C. Atmospheric Corrosion
B. XPS
C. Oxidation
C. Passive Films

ABSTRACT

The protection offered by graphene to copper mono- and polycrystals is studied. Cu(1 1 1) surface shows no traces of corrosion products due to the graphene coating. At the same time copper oxides are found on the copper polycrystalline foil despite the protection due to electrolyte intercalation at the graphene/copper interface. However, the amount of corrosion products is still lower in this case than in non-protected copper. The quantitative analysis of corrosion processes are based on XPS and AES spectra of non-coated and coated copper single and polycrystals. We evaluate graphene as a protection against corrosion in regard to industrial applications.

1. Introduction

Corrosion of copper is a major problem of the electronic industry. This metal, in its pure form, exhibits nearly unparalleled electrical and thermal conductivity values [1,2]. Those properties could ensure many applications of copper, such as interconnections, heat sinks or conductive tracks. However, during the exposure of copper surface to ambient atmosphere, a thin layer of oxides is formed in a series of electrochemical reactions [3–7]. The conductive properties of the corrosion products are significantly inferior to those of pure copper, and their presence on the surface drastically influences surface properties of the system [8,9]. In most cases this effectively limits the applicational potential of copper. Impact of the corrosion is especially important in the age of miniaturization of the electronic devices, as the changes in the structure of the surface influence properties of whole device.

There are various methods of controlling the corrosion of copper such as alloying or coating. Application of either of those methods might significantly reduce the scope of changes introduced by corrosion. However, such protection often comes at the price of the exceptional properties of copper – both alloying and coating may increase both electrical and thermal resistivity of copper [10]. Also, in case of coatings, the dimensions of the coated device are increased, as coating layers can have thickness of at least few nanometers. As each of those methods is useful in the narrow range of applications, one needs to put much care when alloying or coating copper.

Recently it has been shown that graphene can serve as impermeable barrier to molecules [11]. Because of this property it has been suggested to serve as the coating for various metals, including copper in both atmospheric and liquid conditions [12–16]. What is also important, graphene shows a degree of chemical inertness, therefore it not only protects the underlying surface, but also its structure remains unchanged during oxidation [17]. Moreover, graphene itself has unusual properties that in many cases cover those of copper. It has an excellent charge carrier mobility [18], thus may have no negative impact on the conductivity of graphene-coated copper devices. It is also excellent thermal conductor [19] and as such may not interfere with thermal properties of copper. As graphene can be easily grown as single or few layers it would not change the dimensions of copper devices. Furthermore, with the CVD method, graphene can be grown directly onto surface of copper, which simplifies the coating process and ensures high coverage [20]. It is also stable in air at the temperatures up to 500 °C [21]. Because of that graphene could prove to be an excellent coating agent for electronic applications of copper.

The CVD graphene grown directly on copper surface is not defect-free, however. Instead of single, continuous layer, it is composed of islands, or domains [22–24]. The barriers between them are usually not continuous or might have high defect density. The breaking of hexagonal symmetry of the lattice of graphene

* Corresponding author. Tel.: +48 42 635 56 94.
E-mail address: iwlasny@uni.lodz.pl (I. Wlasny).

http://dx.doi.org/10.1016/j.corsci.2014.11.027
0010-938X/

may serve as gateways for molecules and ions, thus lead to local corrosive changes in the chemical structure of copper [25]. Furthermore, different faces of copper crystals create different interfaces with graphene layers. In case of (1 1 1) face of Cu, the nearly identical atomic configurations of graphene and Cu(1 1 1) allow for no molecules of atmospheric gases or ions to intercalate between those two materials [26]. Interfaces of graphene and other faces of copper, however, do not inhibit that process in such degree [26].

Despite the fact that graphene-coated (1 1 1) single crystals offer the best corrosion resistance, polycrystalline copper is much more important from the point of view of applications of copper and it is dominant in industry. It is known, however, that the mismatched copper–graphene interface does allow for some degree of electrolyte intercalation between the two materials [27]. This leads to corrosive changes on top of the copper despite the protection. However, the quantitative characterization of this process faced significant difficulties. This is because the polycrystals are non-uniform and can differ in many aspects such as average copper grain size, which might impact the corrosion rate. For these reasons the efficiency of graphene protection for polycrystalline copper requires further investigations.

In this paper we try to address the issue of atmospheric corrosion in graphene-coated copper. We present the comprehensive results of our investigation of the corrosion of protected mono- and polycrystals in ambient conditions and compare the results to non-coated copper. We analyze the chemical structure of the samples after exposing to the atmospheric conditions. After confirming the crystallographic alignment and presence of the graphene layers in coated samples using Low Energy Electron Diffraction (LEED) and Raman Spectroscopy (RS) we investigate the changes in the chemical structure of the surface of the samples with complimentary techniques of Auger Electron Spectroscopy (AES) and X-ray Photoemission Spectroscopy (XPS).

Our investigations focus on assessment of the effectiveness of the protection against atmospheric corrosion in polycrystalline copper with graphene coating in comparison to most protected (1 1 1) surfaces and non-coated copper. We try to determine the importance of corrosion occurring in graphene-coated polycrystalline copper and the impact of this process in industrial applications.

2. Experimental

In this paper we present results of our investigations conducted on three samples. First of them was commercial copper single crystal with (1 1 1) oriented surface. This sample is later referred to as Cu(1 1 1). The second sample, referred to as G/Cu(1 1 1), was also a copper single crystal, however, the surface of the sample was coated with graphene. The sizes of both of those samples were 8 mm × 8 mm × 1 mm. The third sample was 8 mm × 8 mm × 0.2 mm polycrystalline copper coated with graphene. In this article it is referred to as G/Cu_{foil}.

The surfaces of Cu(1 1 1) and G/Cu(1 1 1), prior to coating with graphene, were prepared by electrochemical polishing to ensure desired orientation of the surfaces of the crystals. Subsequently all of the surfaces, including the substrate of G/Cu_{foil}, were cleaned under H_2/Ar gas flow at the pressure of 100 mbar at 1000 °C. Those conditions allowed for the contamination to desorb from the surfaces and for the reduction of the copper oxides formed by the corrosion that might have occurred beforehand.

The graphene coatings in G/Cu(1 1 1) and G/Cu_{foil} samples were created with Chemical Vapor Deposition (CVD) method using a commercial horizontal CVD hot-wall reactor (Aixtron VP508), which is inductively heated with an RF generator, using propane (C_3H_8) gas as a precursor which was mixed with H_2 to limit sublimation of copper [28].

After the preparation of the samples, the Raman spectroscopy measures were conducted. Spectra were taken with Renishaw InVia spectrometer with 100× objective and 532 nm Nd:YAG laser light source.

All of the samples were exposed to the urban atmospheric conditions to enable the reactions of the corrosion. The influence of external phenomena, such as dust or wind, was minimized by a glass barrier. The exposure lasted 20 days. During that time the samples were held at the temperature of about 18–20 °C and atmospheric pressure. Humidity was close to 25%. During the exposure the amounts of NO_x species were estimated to about 24.7 μg/m^3 (including NO – 3.9 μg/m^3 and NO_2 – 18.6 μg/m^3), SO_2 to 9.3 μg/m^3 and CO to 457 μg/m^3.

After the mentioned exposure samples were analyzed in Ultra High Vacuum (UHV) conditions at pressure of $2 \cdot 10^{-10}$ mbar at room temperature in Omicron GmbH Multiprobe P system. LEED measurements were conducted with OCI LEED BDL800IR instrument. XPS and AES spectra were taken using Omicron NanoTechnology GmbH EA 125 hemispherical analyzer. XPS spectra were gathered with 0.05 eV step. The energy resolution of the analyzer was $\Delta E_A \approx 0.60$ eV. Non-monochromated Mg Kα (1253.6 eV, FWHM = 0.7 eV) radiation, generated with Omicron NanoTechnology GmbH DAR 400 source was used. For such parameters the resolution of XPS measurements (measured peak width) was close to $\Delta E_M \approx 1$ eV. In case of AES step of the spectra was 0.5 eV and the analyzer energy resolution was $\Delta E_A \approx 0.15$ eV. 3 keV electron beam was generated with Omicron NanoTechnology GmbH EKF 300 source. The size of the spot was 500 μm.

3. Results and discussion

To verify starting parameters of the test samples we identified the crystallographic structure and the presence of graphene in the investigated samples. For that purpose we used LEED and RS techniques, the latter was conducted only on graphene-coated samples.

The LEED pattern of Cu(1 1 1) sample is shown in Fig. 1(a). It consists of six spots forming a hexagon around zero-order diffraction point. It originates from the lattice of (1 1 1) surface of copper crystal [29].

The diffraction pattern of G/Cu(1 1 1) sample is presented in Fig. 1(b). It is significantly different from that of Cu(1 1 1). Three sets of spots are visible, indicated by the red and blue hexagons. The inner, red hexagon corresponds to the surface of copper. The outer spots are connected by a ring, the presence of which indicates that there is a degree of disorder in the orientation of graphene domains in the coating [26,30]. Two of the orientations are favored because of the influence of the lattice of the substrate on the growth of the CVD graphene [31].

The structure of the LEED pattern of G/Cu_{foil}, as seen in Fig. 1(c) is different from the previous samples. The pattern of the copper substrate is not visible. All of the symmetrical features of the image correspond to the graphene coating. As was the case for G/Cu(1 1 1), here we also see the ring indicating the disorder in the graphene domain orientations. In the pattern of G/Cu_{foil} we can also see that there are three preferred orientations of the graphene domains rotated relative to each other by 7°. Such configurations were also observed by other groups [32]. We believe that those may suggest that areas where coating is thicker than single atomic layer might be present.

The Raman spectra of G/Cu(1 1 1) and G/Cu_{foil} are shown in Fig 1(d). The presence of both G and 2D peaks confirm graphitic carbon presence on surface of both samples. The 2D/G intensity ratio is

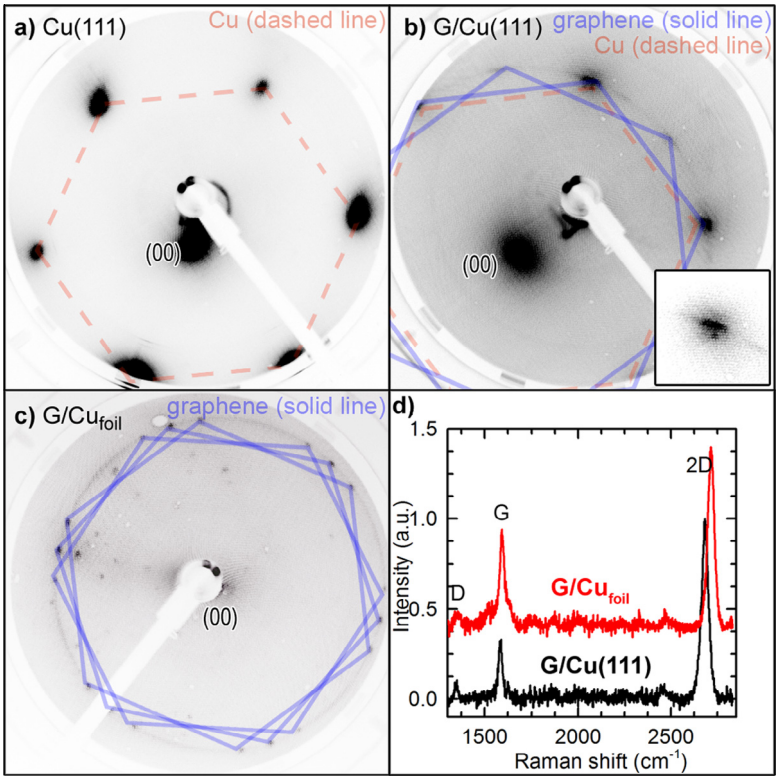

Fig. 1. LEED patterns of (a) Cu(1 1 1), (b) G/Cu(1 1 1), (c) G/Cu$_{foil}$ with visible features of copper (indicated by red hexagons) and graphene (blue hexagons) and (d) Raman spectra of G/Cu(1 1 1) (bottom, black line) and G/Cu$_{foil}$ (top, red line). (For interpretation of the references to color in this figure legend, the reader is referred to the web version of this article.)

close to 3 and 2 for the G/Cu(1 1 1) and G/Cu$_{foil}$ respectively. The I(2D)/I(G) value for G/Cu(1 1 1) suggests that one is predominantly dealing with single graphene layer [33]. The positions of G and 2D lines for G/Cu(1 1 1) are 1584 cm^{-1} and 2683 cm^{-1} respectively, which is close to a free standing graphene monolayer. On the other hand positions of G and 2D lines for G/Cu$_{foil}$ are 1593 cm^{-1} and 2720 cm^{-1}, which indicate a relatively large strain.

After confirming the structure of the investigated samples we proceed to chemical analysis of the samples after exposing them to ambient atmosphere for 20 days. At first we conducted AES and XPS experiments on Cu(1 1 1) sample. As this sample has no protection from corrosion, the results will later serve as a reference point for the changes seen on other samples. This was crucial for our experiment, as the corrosion of copper is heavily dependent on the environmental conditions, such as temperature, pressure and composition of atmosphere [3]. By establishing that all of the samples were held in the same conditions we ensure that the only two factors that cause the changes between the samples are the presence of the coating and the structure of the substrate of graphene.

The AES investigations of Cu(1 1 1) sample, as seen in Fig. 2(a) indicate presence of three elements. First of those is Cu indicated by the presence of Cu LVV, LMV and LMM peaks [34], the presence of which is expected, as products of all reactions of copper with atmospheric gases at room temperature contain copper atoms. The second most intensive peak of the spectrum is O KVV, which indicates presence of the oxygen [34]. While it might originate from the contamination physisorbed from the air, its intensity suggests that it is mostly tied to the presence of copper oxides on the surface of the samples. This is confirmed by a closer look at the Cu LVV peak (Fig. 2(b)). Here one can see that the spectrum has features of either Cu, CuO or both, which cannot be differentiated due to limitations in spectrometer resolution, component with

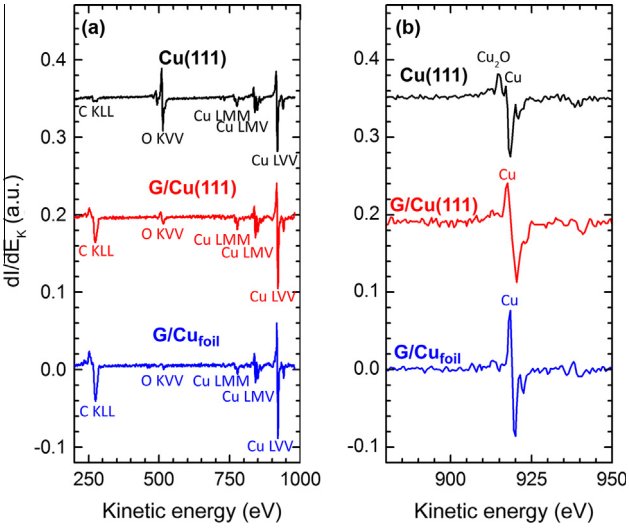

Fig. 2. (a) High energy range AES spectra and (b) Cu LVV AES spectra of Cu(1 1 1) – black line, G/Cu(1 1 1) – red line and G/Cu$_{foil}$ – blue line. (For interpretation of the references to color in this figure legend, the reader is referred to the web version of this article.)

maximum at about 918 eV is seen, and of Cu_2O – component with local maximum at about 916 eV [34].

The copper(I) oxide is the corrosion product with the highest creation rate during the early stages of corrosion of copper in air at room temperatures. It is created in the series of electrochemical reactions, which can be written in simplified form (1) [4].

$$4Cu + O_2 \rightarrow 2Cu_2O \quad (1)$$

Also, carbon was detected on the surface. Again, this might be due to pollutants from the air, however, carbon is also present in one of the products of the corrosion – copper(II) carbonate. It is not possible, however, to confirm its presence with AES only.

To investigate the composition of Cu(1 1 1) surface more closely we used the XPS technique. The XPS Cu $2p_{3/2}$ spectrum of Cu(1 1 1) sample is seen in Fig. 3(a). One can easily see that the analyzed peak (black line) is heavily asymmetrical and has complex structure. Deconvolution indicates that at least three copper species are present as we have found three composite Gauss–Lorentz type curves, with their local maxima at 932.6 eV, 933.7 eV and 935.1 eV. The first component (red line) is associated with both pure copper and Cu_2O, which have similar binding energies [35] and thus are not distinguishable. While it does not clearly indicate the presence of Cu_2O, the previously described analysis of Cu LVV Auger peak confirms the presence of the copper(I) oxide created in reaction (1). The second component (purple line) signifies presence of the CuO on the surface of Cu(1 1 1) [35]. This oxide is the secondary product of the corrosion reactions, as at room temperatures it is created from the reaction of Cu_2O with oxygen (reaction (2)) [36].

$$2Cu_2O + O_2 \rightarrow 4CuO \quad (2)$$

The last component (green line) confirms presence of copper(II) hydroxide and copper(II) carbonate [25], which, as was the case for the first component, both have similar binding energies, and were not distinguishable. The copper(II) hydroxide is always created during the copper corrosion, as it is result of reaction of copper and hydroxyl ions (3) [4], both of which are required for the electrochemical corrosion of copper to take place [3].

$$Cu^{2+} + 2OH^- \rightarrow Cu(OH)_2 \quad (3)$$

Copper(II) carbonate formation, however, is dependent on atmospheric composition and as seen in reaction (4) requires presence of carbon dioxide in the atmosphere.

$$Cu^{2+} + CO_2 + H_2O \rightarrow CuCO_3 + 2H^+ \quad (4)$$

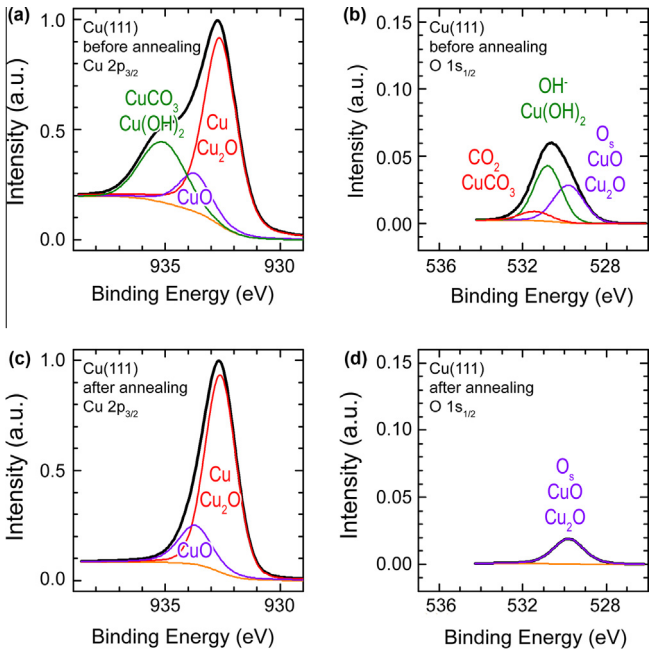

Fig. 3. (a) Cu $2p_{3/2}$ and (b) O $1s_{1/2}$ spectra of Cu(1 1 1) before annealing, (c) Cu $2p_{3/2}$ and (d) O $1s_{1/2}$ spectra of Cu(1 1 1) after annealing at 300 °C in 20 min in UHV conditions.

While the process is not occurring fast due to (1 1 1) orientation of the surface of our sample, we observed certain degree of roughness due to the polishing which introduces defect sites and local deviations from the (1 1 1) orientation of the surface, thus the reaction (4) might have been enabled.

The analysis of O $1s_{1/2}$ peak is in agreement with the previously described observations. The deconvolution of the oxygen XPS peak revealed that it also is composed of three curves, which is seen in Fig. 3(b). First one (purple line) has local maximum at 529.7 eV. This component is associated with oxygen in both of the oxides of copper [37]. However, it may also denote surface oxygen, which is physisorbed on the surface of the sample. The second component (530.7 eV, green line) indicates presence of $Cu(OH)_2$ as well as the hydroxyl ions [37]. As it was mentioned earlier, the presence of the latter is a requirement for the electrochemical corrosion. The last curve (red line) is associated with carbon dioxide and copper(II) carbonate [37]. As the carbon dioxide presence may be leading to the formation of $CuCO_3$ it is possible that this compound is present on the surface, which may explain the presence of C KLL peak in the AES spectrum of the sample (see Fig. 2(a)).

As each of the components in analyzed spectra may have different interpretations we deemed it necessary to confirm that sought compounds were present in the samples. To do so we used the fact that at the elevated temperatures (over 290 °C) the balance between each of the corrosion products shifts and their formations rates change. One of those processes is the acceleration of the oxidation of Cu_2O into CuO (reaction (2)) [6,5].

Furthermore, both $CuCO_3$ and $Cu(OH)_2$ convert to CuO in the processes described by reactions (5) and (6) [5].

$$Cu(OH)_2 \rightarrow CuO + H_2O \quad (5)$$

$$CuCO_3 \rightarrow CuO + CO_2 \quad (6)$$

Those processes are vital, as they indicate that while low-temperature annealing might lead to desorption of weakly bound contamination from the surface, it does not lead to the reduction of copper. Also, it leads to the dominance of CuO as the main corrosion product of copper.

To induce aforementioned changes we annealed the Cu(1 1 1) sample in the UHV condition at 300 °C for 20 min. As seen in Fig. 3(c), there were changes in bonds the copper atoms were forming, which are in agreement with our predictions. The major difference between the peak before and after annealing is the complete disappearance of $Cu(OH)_2/CuCO_3$ component. Also, as those compounds decompose to CuO [5], it was expected that the CuO component increased its intensity relative to Cu/Cu_2O curve. The changes also have an influence on O $1s_{1/2}$ spectrum (Fig. 1(d)). In this case two of the components disappeared. This is related to aforementioned decomposition of copper(II) hydroxide and copper(II) carbonate, but also to evaporation of the electrolyte layer, the presence of which is the perquisite of the electrochemical corrosion, and carbon dioxide. The remaining component can be related to both of the copper oxides and the oxygen adsorbates [37]. However, in the latter case it is likely those species would also evaporate. Thus we assume that the entirety of the O 1s spectrum is associated with copper oxides only (Fig. 3(d)).

The estimation of the total area of Cu $2p_{3/2}$ and O $1s_{1/2}$ peaks gives rough relative amounts of the concentration of those elements in the surface of Cu(1 1 1) sample. Before the sample was subjected to the thermal treatment the atomic percentages of copper and oxygen 79% and 21%, which are calculated based on the relative intensities of the peaks. After the annealing procedure the values changed to 96% and 4%. As the conditions during annealing (300 °C, UHV) do not allow for reduction of copper–oxygen compounds the change is associated with desorption of the contamination as well as the electrolyte layer. As after the thermal treatment

of the sample the oxygen on the surface is associated with the corrosion products only, the area ratio of the samples after the annealing seem to be good indicator of the rate of the corrosion.

As we identified the corrosion of copper under certain conditions we can proceed with analyzing the corrosion of graphene-coated copper. The first case of such system is Cu(1 1 1) crystal coated with monolayer graphene. The AES spectrum of G/Cu(1 1 1) is seen in Fig. 2(a). Compared to spectrum of Cu(1 1 1) quantity of the oxygen in the surface is much lower. This difference originates from the fact that the graphene coating disables access of the air and electrolytes to copper [14,38]. The Cu LVV spectrum of G/Cu(1 1 1) (see Fig. 2(b)) does not have visible component at 916 eV, suggesting no oxides were formed on the surface of the sample, however, as Auger spectrum of copper is complex, which makes it difficult to deconvolute and estimate presence of Cu_2O, as was the case for Cu(1 1 1), we conducted XPS experiment on G/Cu(1 1 1) as well.

The analysis of Cu $2p_{3/2}$ peak, as seen in Fig. 4(a) suggests no copper oxides are present on the surface of G/Cu(1 1 1). The peak was deconvoluted with single Gauss–Lorentz curve, with local maximum at 932.7 eV, which corresponds to Cu and Cu_2O [35]. However, it is unlikely that the copper(I) oxide would occur without other corrosion products, especially copper(II) oxide [3]. Initial analysis of O $1s_{1/2}$ peak shows that some oxygen species are present. The deconvolution (Fig. 4(b)) suggests that at least three different oxygen species can be found. It is difficult to identify them, however, as after annealing the O $1s_{1/2}$ peak disappears completely, as seen in Fig. 4(d). At the same there are no changes in the Cu $2p_{3/2}$ spectrum (Fig. 4(c)). The behavior of the XPS spectra of G/Cu(1 1 1) is understandable considering presence of the contamination of the sample, which was a result of the exposure to the atmosphere. During the exposure the contamination, which contained oxygen species, settled on the surface of the sample, leading to appearance of oxygen species in AES and XPS spectra. As they were bound weakly they desorbed in 300 °C [39]. There were no oxygen species found afterwards, therefore we can assume that no corrosion of copper occurred in the copper in G/Cu(1 1 1) due to graphene coating. This is not true, however, as our previous research [25] show that there are traces of corrosion present in the proximity of graphene discontinuities. This mechanism can eventually lead to accelerated corrosion due to high electrical conductance of graphene [40–42]. However, the influence of graphene defects might be controlled to some extent by multiple coating or introduction of chemical reactants [38,42].

The contribution of this mechanism towards the corrosion of the copper substrate in this case is slight and the amount of oxides formed is too low to be detectable by XPS and AES after twenty days of exposure.

The last stage of our investigation is the study of the corrosion of the graphene-coated polycrystalline copper (sample G/Cu_{foil}). As the corrosion stemming from the discontinuities of the graphene coating is not seen in the XPS, the most probable mechanism that can lead to the observed corrosion of the graphene-coated copper polycrystal is the intercalation of electrolyte at the interfaces of graphene faces of copper other than (1 1 1). However, just as was the case in G/Cu(1 1 1) the AES investigations of G/Cu_{foil} shows only slight presence of the oxygen (Fig. 2(a)). Actually the intensity of O KVV peak of the sample is lower than that of G/Cu(1 1 1). It can be attributed to either higher coverage of the surface with the graphene or the lesser rate of the adsorption of the impurities from the ambient air. The investigations of Cu LVV peak shows no Cu_2O component, as seen in Fig. 2(b). This suggests that, in this sample corrosion was slowed down significantly, despite the enabled intercalation at the graphene–copper interface.

While the AES spectra of the G/Cu_{foil} does not indicate unequivocally that any noticeable corrosion occurred at the surface or the interface between the graphene and the substrate, the XPS spectra in Fig. 5 indicate higher rate of the interaction of the copper and the air molecules than in G/Cu(1 1 1) system. The difference between Cu $2p_{3/2}$ peaks of G/Cu(1 1 1) (Fig. 4(a)) and G/Cu_{foil} (Fig. 5(a)) are slight, but noticeable. Because of this we fit the line with two components instead of one. The additional component peak (purple line) is located at 933.7 eV and can be identified as CuO [35]. While this oxide is not the dominating one in the early

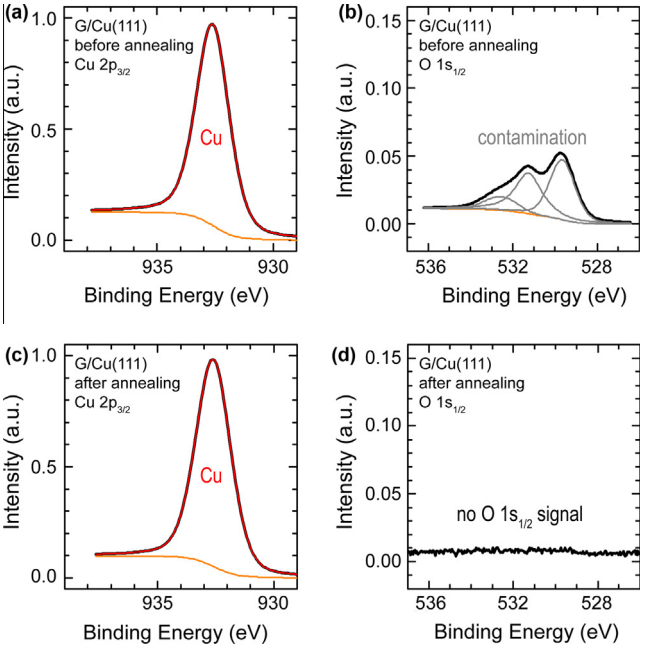

Fig. 4. (a) Cu $2p_{3/2}$ and (b) O $1s_{1/2}$ spectra of G/Cu(1 1 1) before annealing, (c) Cu $2p_{3/2}$ and (d) O $1s_{1/2}$ spectra of G/Cu(1 1 1) after annealing at 300 °C in 20 min in UHV conditions.

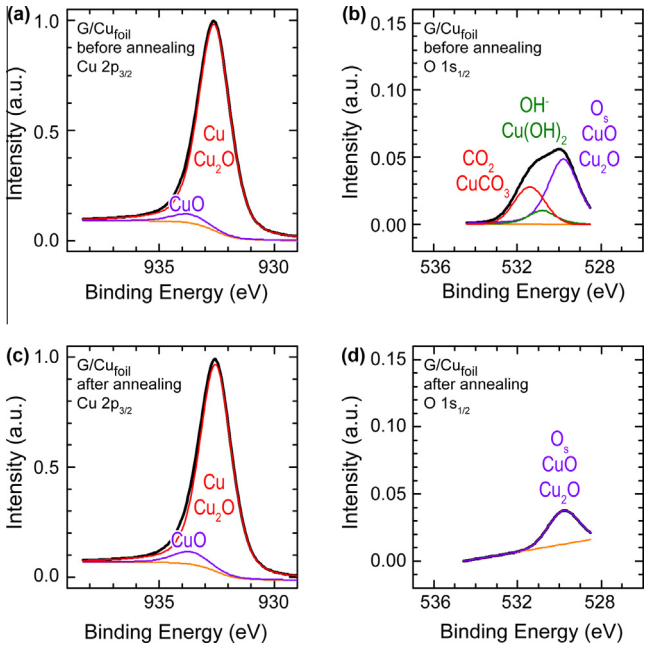

Fig. 5. (a) Cu $2p_{3/2}$ and (b) O $1s_{1/2}$ spectra of G/Cu_{foil} before annealing, (c) Cu $2p_{3/2}$ and (f) O $1s_{1/2}$ spectra of G/Cu_{foil} after annealing at 300 °C in 20 min in UHV conditions.

stages of the corrosion of copper it can be used as an indicator of the corrosion reactions, as unlike the peak of Cu_2O it does not overlap pure Cu. Neither $Cu(OH)_2$ nor $CuCO_3$ are found.

The interpretation of the Cu $2p_{3/2}$ peak seems confirmed by the analysis of O $1s_{1/2}$ spectrum of G/Cu_{foil} (Fig. 5(b)). As was the case of Cu(1 1 1) (Fig. 3(b)), the peak is composed of three component curve suggesting presence of CuO, Cu_2O, hydroxyl ions or $Cu(OH)_2$ and either carbon dioxide or $CuCO_3$. Small ratio of the intensities of first two components proves that there is much less of the hydroxyl groups in the surface, suggesting slower rate of the diffusion of hydroxyl ions on the copper/graphene interface. The $CO_2/CuCO_3$ component can be most likely attributed to the graphene defects or the contamination of the sample.

The thermal treatment of G/Cu_{foil} sample introduces some changes in the XPS spectra. As expected the ratio between CuO and Cu/Cu_2O components in Cu $2p_{3/2}$ peak is shifted as seen in Fig. 5(c). This is explained by the decomposition of the copper(II) carbonate and copper(II) hydroxide into CuO [5]. The CuO/Cu_2O component of O $1s_{1/2}$ (Fig. 5(d)) shows slight decrease in the intensity after annealing, while the other components disappeared completely. This should not be understood as a decrease in the relative volume of the oxides in the substrate. As was shown in the case of G/Cu(1 1 1) the oxygen species from the contamination are seen before annealing, which are removed during the process. This contributes to the error in the estimation of the relative volumes of the oxides before annealing. As such we can use the Cu $2p_{3/2}$ and O $1s_{1/2}$ peaks after the annealing as the indicator and the gauge of the corrosion in the graphene-coated copper systems. In this case the atomic percentages of copper and oxygen were equal to 99.5% and 0.5%, which suggest that the corrosion is much slower in the polycrystalline copper due to the graphene coating, but is not disabled completely.

4. Conclusion

In summary we have investigated the early stages of corrosion of graphene-coated copper mono- and polycrystalline substrates. Our results clearly indicate that while the corrosion is not seen in the copper single crystal due to the graphene coating, it is not the case for the polycrystalline materials, which are the most common in the industry. For polycrystals, despite the graphene protection, the corrosion was enabled due to the intercalation of the electrolyte in the graphene/copper interface. Observed rate of corrosion in case of the graphene-protected polycrystal was noticeably high. In our opinion this shows that described phenomena cannot be overlooked in the industrial applications. In particular, our results show that it is vital to carefully estimate the lifetime of the devices based on the graphene-coated polycrystalline copper.

Acknowledgements

This work was financially supported by the National Center for Research and Development Projects GRAF-TECH/NCBR/15/25/2013 "GRAPH-PRINT" and GRAF-TECH/NCBR/01/32/2012 "GRAFMET", by the National Science Centre under the Project DEC-2012/05/B/ST5/00354 and by the University of Lodz (Grant supporting young scientists). The research has also received funding from the European Union Seventh Framework Programme under Grant agreement n°604391 Graphene Flagship. P. Dabrowski was supported by Polish National Science Centre under the DEC-2012/04/S/ST3/00186 project.

Appendix A. Supplementary material

Supplementary data associated with this article can be found, in the online version, at http://dx.doi.org/10.1016/j.corsci.2014.11.027.

References

[1] D.J. Griffiths, Introduction to Electrodynamics, fourth ed., Addison-Wesley, 2012.
[2] R.A. Serway, J.W. Jewett, Principles of Physics: a Calculus-Based Text, second ed., Cengage Learning, 1992.
[3] S. Syed, Atmospheric corrosion of materials, Emirates J. Eng. Res. 11 (2006) 1–24.
[4] I. Platzman, R. Brener, H. Haick, R. Tannenbaum, Oxidation of polycrystalline copper thin films at ambient conditions, J. Phys. Chem. C 112 (2008) 1101–1108.
[5] H.W. Richardson, Copper compounds, in: Ullmann's Encyclopedia of Industrial Chemistry, Wiley-VCH, Weinheim, 2000.
[6] Y. Wan, X. Wang, H. Sun, Y. Li, K. Zhang, Y. Wu, Corrosion behavior of copper at elevated temperature, Int. J. Electrochem. Sci. 7 (2012) 7902–7914.
[7] W.L. Masterton, C.N. Hurley, E. Neth, Chemistry: Principles and Reactions, seventh ed., Cengage Learning, 2011.
[8] N. Serin, T. Serin, S. Karadeniz, Current-limiting property of Cu/cupric oxide/Cu sandwich structure, Semicond. Sci. Technol. 17 (2002) 60–64.
[9] A. Parretta, M.K. Jayaraj, A. Di Nocera, S. Loreti, L. Quercia, A. Agati, Electrical and optical properties of copper oxide films prepared by reactive RF magnetron sputtering, Phys. Status Solidi A 155 (1996) 399–404.
[10] C.Y. Ho, M.W. Ackerman, K.Y. Wu, T.N. Havill, R.H. Bogaard, R.A. Matula, S.G. Oh, H.M. James, Electrical resistivity of ten selected binary alloy systems, J. Phys. Chem. Ref. Data 12 (1983) 183–322.
[11] J.S. Bunch, S.S. Verbridge, J.S. Alden, A.M. van der Zande, J.M. Parpia, H.G. Craighead, P.L. McEuen, Impermeable atomic membranes from graphene sheets, Nano Lett. 8 (2008) 2458–2462.
[12] L. Nilsson, M. Andersen, R. Balog, E. Lægsgaard, P. Hofmann, F. Besenbacher, B. Hammer, I. Stensgaard, L. Hornekær, Graphene coatings: probing the limits of the one atom thick protection layer, ACS Nano 6 (2012) 10258–10266.
[13] S. Chen, L. Brown, M. Levendorf, W. Cai, S.-Y. Ju, J. Edgeworth, X. Li, C.W. Magnuson, A. Velamakanni, R.D. Piner, J. Kang, J. Park, R.S. Ruoff, Oxidation resistance of graphene-coated Cu and Cu/Ni alloy, ACS Nano 5 (2011) 1321–1327.
[14] D. Prasai, J.C. Tuberquia, R.R. Harl, G.K. Jennings, K.I. Bolotin, Graphene: corrosion-inhibiting coating, ACS Nano 6 (2012) 1102–1108.
[15] A.S. Kousalya, A. Kumar, R. Paul, D. Zemlyanov, T.S. Fisher, Graphene: an effective oxidation barrier coating for liquid and two-phase cooling systems, Corros. Sci. 69 (2013) 5–10.
[16] N.T. Kirkland, T. Schiller, N. Medhekar, N. Birbilis, Exploring graphene as a corrosion protection barrier, Corros. Sci. 56 (2012) 1–4.
[17] G. Kalita, M.E. Ayhan, S. Sharma, S.M. Shinde, D. Ghimire, K. Wakita, M. Umeno, M. Tanemura, Low temperature deposited graphene by surface wave plasma CVD as effective oxidation resistive barrier, Corros. Sci. 78 (2014) 183–187.
[18] K.I. Bolotin, K.J. Sikes, Z. Jiang, G. Fudenberg, J. Hone, P. Kim, H.L. Stormer, Ultrahigh electron mobility in suspended graphene, Solid State Commun. 146 (2008) 351–355.
[19] A.A. Balandin, Thermal properties of graphene and nanostructured carbon materials, Nat. Mater. 10 (2011) 569–581.
[20] S. Nie, W. Wu, S. Xing, Q. Yu, J. Bao, S.-S. Pei, K.F. McCarty, Growth from below: bilayer graphene on copper by chemical vapor deposition, New J. Phys. 14 (2012) 093028.
[21] H.Y. Nan, Z.H. Ni, J. Wang, Z. Zafar, Z.X. Shi, Y.Y. Wang, The thermal stability of graphene in air investigated by Raman spectroscopy, J. Raman Spectrosc. 44 (2013) 1018–1021.
[22] L.P. Biró, P. Lambin, Grain boundaries in graphene grown by chemical vapor deposition, New J. Phys. 15 (2013) 035024.
[23] Y.H. Zhang, B. Wang, H.R. Zhang, Z.Y. Chen, Y.Q. Zhang, B. Wang, Y.P. Sui, X.L. Li, X.M. Xie, G.H. Yu, Z. Jin, X.Y. Liu, The distribution of wrinkles and their effects on the oxidation resistance of chemical vapor deposition of graphene, Carbon 70 (2014) 81–86.
[24] M. Losurdo, M.M. Giangregorio, P. Capezzuto, G. Bruno, Graphene CVD growth on copper and nickel: role of hydrogen in kinetics and structure, Phys. Chem. Chem. Phys. 13 (2011) 20836–20843.
[25] I. Wlasny, P. Dabrowski, M. Rogala, P.J. Kowalczyk, I. Pasternak, W. Strupinski, J.M. Baranowski, Z. Klusek, Role of graphene defects in corrosion of graphene-coated Cu(1 1 1) surface, Appl. Phys. Lett. 102 (2013) 111601.
[26] A.L. Walter, S. Nie, A. Bostwick, K.S. Kim, L. Moreschini, Y.J. Chang, D. Innocenti, K. Horn, K.F. McCarty, E. Rotenberg, Electronic structure of graphene on single-crystal copper substrates, Phys. Rev. B 84 (2013) 195443.
[27] P.R. Kidambi, B.C. Bayer, R. Blume, Z.J. Wang, C. Baehtz, R.S. Weatherup, M.C. Willinger, R. Schloegl, S. Hofmann, Observing graphene grow: catalyst–graphene interactions during scalable graphene growth on polycrystalline copper, Nano Lett. 13 (2013) 4769–4778.
[28] W. Strupinski, K. Grodecki, A. Wysmolek, R. Stepniewski, T. Szkopek, P.E. Gaskell, A. Gruneis, D. Haberer, R. Bozek, J. Krupka, J.M. Baranowski, Graphene epitaxy by chemical vapor deposition on SiC, Nano Lett. 11 (2011) 1786–1791.
[29] V. Matolín, J. Libra, I. Matolínová, V. Nehasil, L. Sedlácek, F. Šutara, Growth of ultra-thin cerium oxide layers on Cu(1 1 1), Appl. Surf. Sci. 254 (2007) 153–155.
[30] K. Wondong, Y. Kwonjae, K.S. Eun, J.K. Sung, H. Chanyong, Scanning tunneling microscopy study on a graphene layer grown on a single-crystal Cu(1 1 1) surface by using chemical vapor deposition, J. Korean Phys. Soc. 59 (2011) 71–74.

[31] M. Batzill, The surface science of graphene: metal interfaces, CVD synthesis, nanoribbons, chemical modifications, and defects, Surf. Sci. Rep. 67 (2012) 83–115.
[32] L. Gao, J.R. Guest, N.P. Guisinger, Epitaxial graphene on Cu(1 1 1), Nano Lett. 10 (2010) 3512–3516.
[33] A.C. Ferrari, J.C. Meyer, V. Scardaci, C. Casiraghi, M. Lazzeri, F. Mauri, S. Piscanec, D. Jiang, K.S. Novoselov, S. Roth, A.K. Geim, Raman spectrum of graphene and graphene layers, Phys. Rev. Lett. 97 (2006) 187401.
[34] D. Tahir, S. Tougaard, Electronic and optical properties of Cu, CuO and Cu_2O studied by electron spectroscopy, J. Phys.: Condens. Matter 24 (2012) 175002.
[35] K.L. Chavez, D.W. Hess, A novel method of etching copper oxide using acetic acid, J. Electrochem. Soc. 148 (2001) G640–G643.
[36] P.B. Rasmussen, P.A. Taylor, I. Chorkendorff, The interaction of carbon dioxide with Cu(1 0 0), Surf. Sci. 269–270 (1992) 352–359.
[37] X. Deng, A. Verdaguer, T. Herranz, C. Weis, H. Bluhm, M. Salmeron, Surface chemistry of Cu in the presence of CO_2 and H_2O, Langmuir 24 (2008) 9474–9478.
[38] M. Topsakal, H. Şahin, S. Ciraci, Graphene coatings: an efficient protection from oxidation, Phys. Rev. B 85 (2012) 155445.
[39] J.H. Warner, F. Schaffel, M. Rummeli, A. Bachmatiuk, Graphene: Fundamentals and Emergent Applications, Elsevier, 2012.
[40] M. Schriver, W. Regan, W.J. Gannett, A.M. Zaniewski, M.F. Crommie, A. Zettl, Graphene as a long-term metal oxidation barrier: worse than nothing, ACS Nano 7 (2013) 5763–5768.
[41] F. Zhou, Z. Li, G.J. Shenoy, L. Li, H. Liu, Enhanced room-temperature corrosion of copper in the presence of graphene, ACS Nano 7 (2013) 6939–6947.
[42] L. Nilsson, M. Andersen, B. Hammer, I. Stensgaard, L. Hornæker, Breakdown of the graphene coating effect under sequential exposure to O_2 and H_2S, J. Phys. Chem. Lett. 4 (2013) 3770–3774.